Soft lubrication: A generalized numerical methodology

Soft lubrication: a generalized numerical methodology

Carmine Putignano*

Department of Mechanics, Mathematics and Management,Politecnico di Bari, Bari, Italy.

Abstract

A generalized numerical methodology is introduced to deal with the lubrication between soft solids exhibiting linear viscoelastic rheological properties. By means of this approach, it is shown that significant deviation from classic elasto-hydrodynamic theory occur in terms of film thickness, pressure distribution and friction. By focusing on a simple tribo-system, consisting in a sphere in contact with a layer, the influence of the contact configuration is investigated. Ultimately, viscoelastic lubrication is shown to be exhaustively governed by three parameters: the Hersey number and the two contacting solids dimensionless velocities. Finally, numerically obtained friction values are compared with experiments to validate the methodology.

Keywords: viscoelasticity, friction, lubrication, film thickness, soft matter.

1. Introduction

In the past decade, soft lubrication has emerged as a crucial field in applied mechanics and, specifically, tribology research. Indeed, a countless number of investigations, relying on analytical, numerical and experimental approaches, has been aimed at understanding what occurs when two soft bodies, properly lubricated by a fluid, come into contact (1)(2). The reasons for such an intense interest is directly related to the large variety of systems, where soft lubrication is the fundamental governing mechanism (3)(5)(4)(6). Certainly, an important class of soft structures under lubricated conditions is found in biomechanics: soft bio-lubrication is ubiquitous in our body as it

*Corresponding author. Phone: +39 080 596 2711
Email address: carmine.putignano@poliba.it (Carmine Putignano)

occurs at different scales and in several systems, including cells, organs and tissues (7)(8). As an example at the macro-scale, let us recall that human fingertip grasping and gripping are dramatically governed by the amount of liquid at the contact interface: this is extremely critical in the touchscreens Era we are currently living (9)(10). On the other hand, we should not underestimate the importance that soft lubrication has currently in industry. Indeed, a slow, but continuos shift from metals to polymers has been occuring in the last decades, given the cheaper cost, the lighter weight and the environmental compatibility offered by rubber-based materials and composites. Rubber bearings, seals, spacers, dampers are only possible examples of soft mechanical components (11)(12)(13)(14)(15). Furthermore, at smaller scales, soft lubrication plays a crucial role in determining the operation and the dynamics of micro- and nano-actuators (16).

Such a marked applicative interest is intrinsically linked to the theoretical complexity of the theme. Indeed, soft matter exhibits a non-linearly elastic and, often, time-dependent constitutive behaviour: this makes hard to develop effective theoretical models (17). Things become even more complicated when soft bodies are involved into a lubricated contact: the presence of different phases, including gases and fluids, determines strong coupling effects to be accounted for in a complex multi-physics simulation environment (1). Furthermore, the presence of roughness on the solids into contact exacerbates the problem intricacy as it introduces a large range of space and, thus, time scales to be considered (18)(19).

The complexity of such a scenario has, thus, required the aforementioned research efforts: by inferring data from tribological experiments or numerical simulations, these have been aimed at obtaining relations between pressure distribution, film thickness and, ultimately, friction (1). However, only very recently, an aspect of dramatic importance has started to attract the proper consideration it deserves. This is related to the soft materials rheology, which is time-dependent and can be often modelled as viscoelastic (20)(21)(22)(23). The poor consideration of the influence of solid viscoelasticity on lubrication is somehow surprising, given the large number of investigations dedicated, conversely, to the dry viscoelastic contact mechanics. Analytical (24; 11), numerical (25)(26)(31)(32) and experimental (27; 28) studies have been proposed to point out aspects related to contact area, stiffness and, ultimately, hysteretic friction. However, in Ref. (21), it has been shown that viscoelasticity does really play a significant role in lubricated conditions as much as in the dry case. Specifically, there occur dramatic changes in the pressure

and the thickness distributions; as a consequence, the friction/speed curve shows a marked deviation from the trend predicted by the Stribeck relation classically formulated in lubrication science.

In this paper, we generalize the approach proposed in Ref. (21) to consider different contact configurations and show how viscoelasticity works differently in each case. As shown in Figure 1, without loss of generality, we focus on a simple yet explicative tribo-system, i.e., a ball rolling over a disk. Incidentally, such a scheme describes a ball-on-disk tribometer and is, therefore, of particular importance in Tribology. Three different configurations are investigated. In the hard-on-soft configuration (HS), the ball is hard and the disc is soft. In the soft-on-hard configuration (SH), the ball is soft and the disc is hard. Finally, in the soft-on-soft configuration (SS), both the ball and the disc are soft. As well known, in purely linear elastic conditions, no difference would be observed in the three cases, but, if the bodies are viscoelastic, dramatic changes have to be expected. Here, we propose a novel numerical methodology to consider the three aforementioned configurations and to account for the different speed values respectively assumed by the ball and the disk. We focus on the film thickness and the pressure distribution, showing the main peculiarities in comparison with classic EHL results. Finally, we propose a comparison, in terms of frictional force, between the numerical outcomes of our methodology and some experimental data recently proposed in literature (23).

2. Mathematical formulation

When dealing with lubrication of deformable bodies, it is necessary to solve, at the same time, the Reynolds equations and the elastic (or viscoelastic) problem governing the deformation experienced by the interacting pair into contact. Indeed, the two aspects are strongly coupled: the displacement of the solid surfaces determines the lubricating film and, consequently, the solution of the Reynolds equations, which govern, on their turn, the pressure distribution and, thus, the solid deformation field. Ultimately, the complete solution of the lubrication problem requires the determination of two unknown distributions, i.e., the film thickness in the contact region and the normal interfacial stress.

Let us start with the geometrical definition of the system. As sketched in Figure 2, a punch clamped in its center rolls, with a peripheral velocity $\mathbf{v}_b$, over a layer sliding with a constant speed $\mathbf{v}_d$. Both the solids are de-

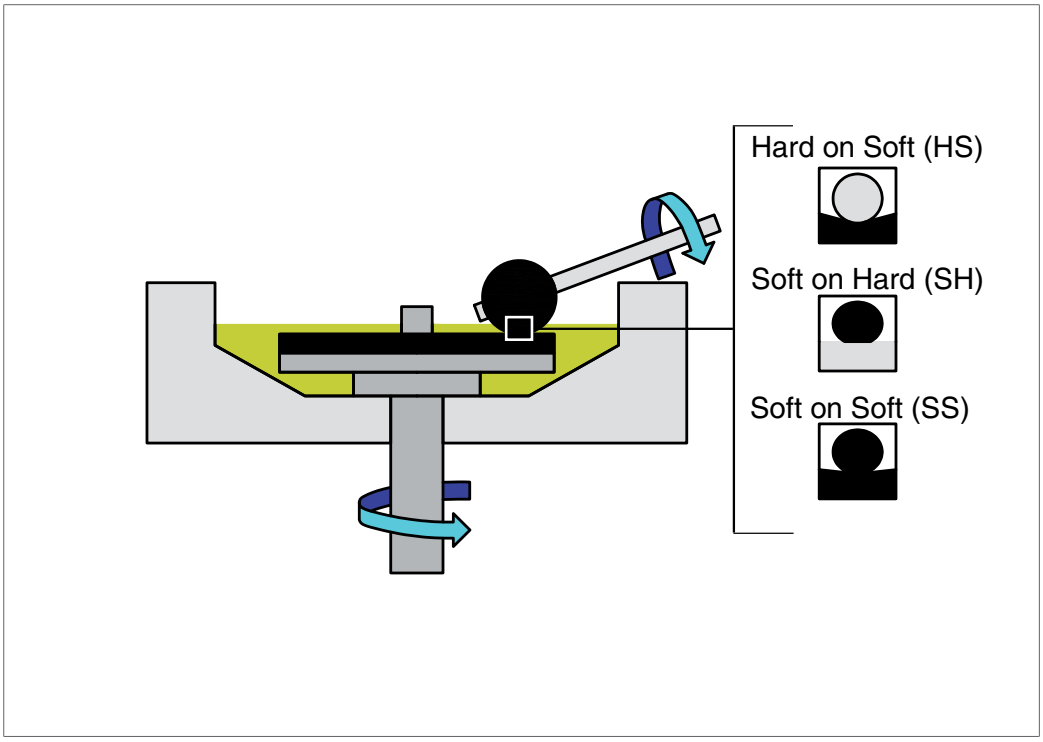

Figure 1: Schematic of the tribo-system under investigation. Three different configurations area considered: hard ball on soft disk (HS), soft ball on hard disk (SH) and soft ball on soft disk (SS).

formable and, specifically, linearly viscoelastic. As for the velocities, given the reference in Figure 2, we assume that there is no spin and, thus, $\mathbf{v}_b$ and $\mathbf{v}_d$ have the same direction, i.e., $\mathbf{v}_b = v_b\mathbf{i}$ and $\mathbf{v}_d = v_d\mathbf{i}$ with $\mathbf{i}$ being the unit vector referred to $x-$axis. At this point, it should be observed that the mathematical formulation under development is totally general and can be applied to any contact configuration, once the geometry of the contacting solids and the velocities $\mathbf{v}_b$ and $\mathbf{v}_d$ are properly defined.

Before focusing in detail on the equations governing film thickness and pressure distribution, it is important to briefly recall how to model, from a mechanical point of view, linear viscoelasticity (39). Indeed, the most general linear viscoelastic model can be encompassed in the following relation:

$$\varepsilon(t) = \int_{-\infty}^{t} d\tau \mathcal{J}(t-\tau)\,\dot{\sigma}(\tau) \tag{1}$$

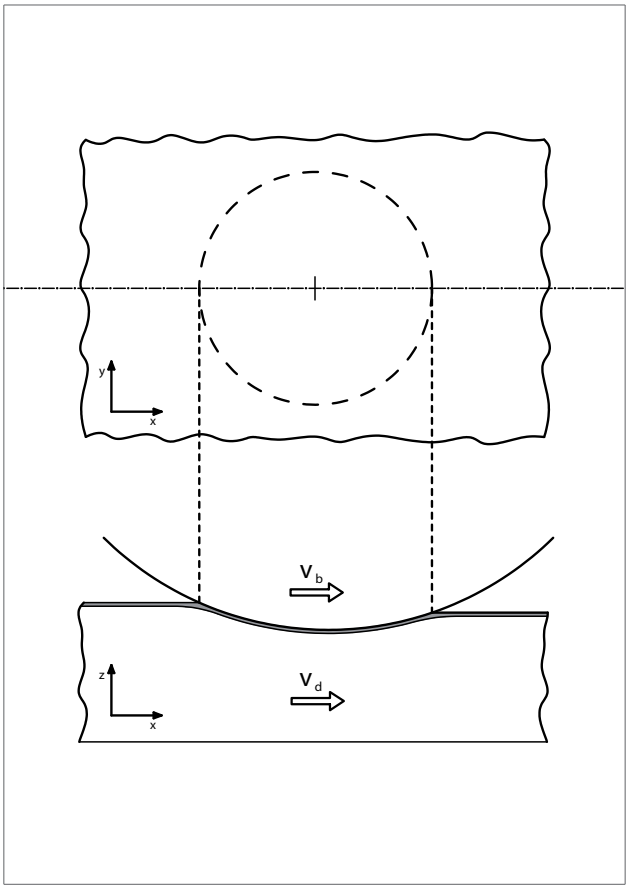

Figure 2: Geometrical definition of the system.

with $\varepsilon(t)$ being the time-dependent strain, $\sigma(t)$ the stress [the symbol '$\cdot$' stands for the time derivative], and the function $\mathcal{J}(t)$ being the creep function. The latter quantity $\mathcal{J}(t)$ must satisfy causality and, therefore, $\mathcal{J}(t<0) = 0$. Furthermore, $\mathcal{J}(t)$ can be related to the material properties by means of the following integral relations (39):

$$\mathcal{J}(t) = \mathcal{H}(t)\left[\frac{1}{E_0} - \int_0^{+\infty} d\tau \mathcal{C}(\tau)\exp(-t/\tau)\right] = \mathcal{H}(t)\left[\frac{1}{E_\infty} + \int_0^{+\infty} d\tau \mathcal{C}(\tau)\exp(-t/\tau)\right] \tag{2}$$

where $\mathcal{H}(t)$ is the Heaviside step function, the real quantities E_0 and E_∞ are respectively the so-called rubbery and glassy elastic moduli, $\mathcal{C}(\tau)$ is a positive

function usually referred to as the creep (or retardation) spectrum (39), and τ is the relaxation time continuously distributed on the real axis. Let us observe that, by writing $\mathcal{C}(\tau) = \sum_k C_k \delta(\tau - \tau_k)$, Eq. (2) can be discretized as $\mathcal{J}(t) = \mathcal{H}(t)\left[1/E_0 - \sum_{k=1}^{n} C_k \exp(-t/\tau_k)\right]$ with C_k and τ_k being respectively the creep coefficients and the relaxation times. Such a discrete form for $\mathcal{J}(t)$ is necessary when featuring any real viscoelastic material.

Furthermore, it is noteworthy to define an additional quantity, that is, the so-called complex viscoelastic modulus of the material $E(\omega)$. Indeed, if we carry out the Fourier transform of Eq. (1) by introducing $\mathcal{J}(\omega) = \int dt \mathcal{J}(t) \exp(-i\omega t)$, $\sigma(\omega) = \int dt \sigma(t) \exp(-i\omega t)$ and $\varepsilon(\omega) = \int dt \varepsilon(t) \exp(-i\omega t)$, we obtain $\varepsilon(\omega) = \sigma(\omega)/E(\omega)$ where $E(\omega)$ is equal to $E(\omega) = [i\omega J(\omega)]^{-1}$. By moving from Eq. (2) , one can easily prove the *sum rule*:

$$\frac{1}{E_0} - \frac{1}{E_\infty} = \frac{2}{\pi} \int_0^\infty d\omega \, \frac{1}{\omega} \mathrm{Im} \frac{1}{E(\omega)} \tag{3}$$

Now, after recalling the fundamentals of linear viscoelasticity, we can focus on the viscoelastic problem for the bodies into contact. As shown in detail in Ref. (25), because of the translational invariance for the geometrical domain and the elastic-viscoelastic correspondence principle (39), in a general linear viscoelastic solid, the linear-viscoelastic relation between the normal surface displacement $u(\mathbf{x}, t)$ and the normal interfacial stress $\sigma(\mathbf{x}, t)$ can be described by means of the following integral equation:

$$u(\mathbf{x}, t) = \int_{-\infty}^{t} d\tau \int d^2x' \mathcal{J}(t - \tau) \mathcal{G}(\mathbf{x} - \mathbf{x}') \dot{\sigma}(\mathbf{x}', \tau), \tag{4}$$

where $\mathbf{x}$ is the in-plane position vector, t is the time, $\mathcal{G}(\mathbf{x})$ and $\mathcal{J}(t)$ are respectively the elastic Green's function and the creep function previously introduced. Incidentally, it should be recalled that, in Eq. (4), the factorization of the integral equation kernel in two terms, that is, $\mathcal{G}(\mathbf{x})$ and $\mathcal{J}(t)$, can be done under the assumption that the solid under study is perfectly homogenous.

Now, if any effect due to a non-uniform temperature field can be neglected, and if both $\mathbf{v}_d$ and $\mathbf{v}_b$ are constant, we are in steady-state conditions and, as shown in detail in Ref. (25), Eq. (4) can be significantly simplified. Specifically, the normal displacement distributions for two bodies, respectively $\mathbf{u}_b$ and $\mathbf{u}_d$, can be estimated as:

$$u_b(\mathbf{x}) = \int d^2x' G_b(\mathbf{x}-\mathbf{x}', \mathbf{v}_b)\,\sigma(\mathbf{x}') \tag{5}$$

$$u_d(\mathbf{x}) = \int d^2x' G_d(\mathbf{x}-\mathbf{x}', \mathbf{v}_d)\,\sigma(\mathbf{x}') \tag{6}$$

The kernel $G_b(\mathbf{x}, \mathbf{v}_b)$ and $G_b(\mathbf{x}, \mathbf{v}_b)$, which depends only parametrically on the sliding speed $\mathbf{v}_b$ and $\mathbf{v}_d$, can be proved to be equal to:

$$G_b(\mathbf{x}, \mathbf{v}_b) = -\frac{1-\upsilon_b^2}{\pi}\left\{\frac{1}{E_{b_\infty}}\frac{1}{|\mathbf{x}|} + \int_0^{+\infty} d\tau \mathcal{C}_b(\tau)\int_0^{+\infty} dz \frac{1}{|\mathbf{x}-\mathbf{v}_b\tau_b z|}\exp(-z)\right\} \tag{7}$$

$$G_d(\mathbf{x}, \mathbf{v}_d) = -\frac{1-\upsilon_d^2}{\pi}\left\{\frac{1}{E_{d_\infty}}\frac{1}{|\mathbf{x}|} + \int_0^{+\infty} d\tau \mathcal{C}_d(\tau)\int_0^{+\infty} dz \frac{1}{|\mathbf{x}-\mathbf{v}_d\tau_d z|}\exp(-z)\right\} \tag{8}$$

Where the quantities υ_b ,E_{b_∞} ,$\mathcal{C}_b$, τ_b and υ_d , E_{d_∞} , $\mathcal{C}_d$, τ_d are respectively the Poisson ratio, the glassy modulus, the creep function and relaxation function respectively for the body on the top and for that one on the bottom, that is, for the ball and the disk in Figure 2.

Let us, now, define the total viscoelastic $u_{tot}(\mathbf{x}) = u_b(\mathbf{x}) + u_d(\mathbf{x})$. It is straightforward to write $u_{tot}(\mathbf{x})$ as:

$$u_{tot}(\mathbf{x}) = \int d^2x' G_{tot}(\mathbf{x}-\mathbf{x}', \mathbf{v}_b, \mathbf{v}_d)\,\sigma(\mathbf{x}') \tag{9}$$

where $G_{tot}(\mathbf{x}-\mathbf{x}', \mathbf{v}_b, \mathbf{v}_d)$ is clearly equal to $G_{tot}(\mathbf{x}-\mathbf{x}', \mathbf{v}_b, \mathbf{v}_d) = G_b(\mathbf{x}-\mathbf{x}', \mathbf{v}_b) + G_d(\mathbf{x}-\mathbf{x}', \mathbf{v}_d)$. In order to be numerically solved, Eq. (9) has to be discretized as a linear system (36; 37). Indeed, this strategy consists in meshing the contact domain in N square cells and, then, assuming that in each square cell the normal stress σ is constant and equal to $\sigma_k = \sigma(\mathbf{X}_k)$, where $\mathbf{X}_k$ is the position vector of the center of the square cell D_k . The normal displacement

at the center of the i-th square cell is $u_i = u(\mathbf{X}_i)$. As shown in detail in Ref. (25), the problem is then reduced to a vectorial linear relation:

$$u_i = L_{ik}(\mathbf{v}_b, \mathbf{v}_d)\,\sigma_k \tag{10}$$

where the response matrix $L_{ik}(\mathbf{v}_b, \mathbf{v}_d)$ parametrically depends on the velocity $\mathbf{v}_d$ and $\mathbf{v}_b$. We observe that the total load acting on the system F_n is equal to $F_n = D_k \Sigma_{k=1}^{N} \sigma_k$ with D_k being the area of each square cell.

Once the solid viscoelastic problem has been reduced to the linear system 10, it is necessary to focus on the equations governing the fluid dynamics of the system. All the assumptions commonly employed when dealing with soft lubrication are considered valid; specifically, we assume no-slip boundary conditions at both solids interface. Let us, then, introduce the Reynolds equations, whose general form can be written as (see Ref. (1; 18)):

$$\frac{\partial \rho h}{\partial t} + \nabla \cdot (\rho h \mathbf{U}) = \nabla \cdot \left(\frac{\rho h^3}{12\eta} \nabla \sigma \right) \tag{11}$$

where $\mathbf{U}$ is the entrainment speed, i.e., the mean surface velocity being equal, for the system in Figure 1, to $\mathbf{U} = (\mathbf{v}_b + \mathbf{v}_d)/2$, ρ is the density (which here is considered constant), η is the fluid viscosity and h is the film thickness. The latter quantity is directly to the total normal displacement u_{tot} and, specifically, $h(x, y) = h_0 + s(x, y) + u_{tot}(x, y)$ with h_0 and $s(x, y)$ being respectively a rigid motion constant and the separation of the contacting surfaces in the undeformed configuration. For the tribo-system studied in this paper and sketched in Figure 1, $s(x, y)$ is equal to $s(x, y) = R - (R - x^2 - y^2)^{1/2}$ with R being the radius of the sphere.

Under the steady-state assumption considered in this study, Equation (11) can be simplified as the time derivative vanishes. Equation (11) is, then, tackled by implementing a finite difference scheme, whose nodes, being equally spaced in the computational domain, correspond to the centers of the boundary elements previously defined for the solid problem. This methodology consists in discretizing the differential terms in Eq. (11) with central differences (1; 18) , thus obtaining the following vectorial equation:

$$h_i = R_{ik}(\mathbf{U}, \mu)\,\sigma_k \tag{12}$$

Ultimately, the problem requires to couple the solid mechanics and fluid dynamics (1; 18; 19) in order to determine the pressure distribution that satisfies, at the same time, both Eq. (10) and Eq. (12). An iterative scheme

is implemented to solve the system formed by the aforementioned vectorial equations. Basically, at each iteration, moving from the film thickness estimation $\tilde{h}_i$ computed at the previous iteration, Eq. (12) is inverted and, thus, an estimated stress field $\tilde{\sigma}_k$ is calculated; $\tilde{\sigma}_k$ is, then, inputted into Eq. (10) in order to compute the new viscoelastic deformation field $\tilde{u}_{i+1}$ and, consequently, the film thickness $\tilde{h}_{i+1}$ for the following iteration. Such an iterative procedure, properly underrelaxed with the Aitken acceleration approach (see e.g. Ref. (18)), keeps on running until film thickness and pressure distributions numerically converge in two consecutive iterations.

Once the lubrication problem is fully solved in terms of pressure distribution and deformations, it is possible to focus on the friction force determined as sum of the viscoelastic hysteretic term (25) and the contribution coming from the fluid losses (1). More in detail, if we recall now that $\mathbf{v}_b$ and $\mathbf{v}_d$ are assumed, without any loss of generality, to be along the x-axis, i.e. $\mathbf{v}_b = v_b\mathbf{i}$ and $\mathbf{v}_d = v_d\mathbf{i}$, by focusing on the solid on the top, that is, the sphere, the friction force F_x can be obtained by adding up the rolling hysteric friction F_r , the Poisseulle contribution F_p and the Couette term F_c, thus leading to:

$$F_x = -\int dAp\frac{\partial h_b}{\partial x} - \int dA\frac{h}{2}\frac{\partial p}{\partial x} + \int dA\eta\frac{(v_d - v_b)}{h} \tag{13}$$

where h_b is the deformed shape of the ball. Consequently, we can define the friction coefficient as $f = |F_x/F_n|$.

Finally, as suggested in Ref. (21), it can be useful to employ dimensionless quantities in the discussion of the results. As for the film thickness h (and, similarly, for all the deformations and quantities defined using units of length), by considering the radius R as characteristic length of the problem, the dimensionless quantity h/R is introduced. Then, by referring to the rubbery elastic modulus E_0 , we define the dimensionless stress distribution σ/E_0 and, consequently, the normal dimensionless load $F_n/\left(R^2E_0\right)$. With regards to the speed, it may be observed that the problem is governed by two time scales: the first one is a characteristic relaxation time τ of the material and the second one is the time employed by each deformable body to cover the length R (25). As a consequence, we define, for the sphere and the disk respectively, the dimensionless speeds $\xi_b = v_b\tau_b/R$ and $\xi_d = v_d\tau_d/R$ with τ_b and τ_d being characteristic relaxation times for the sphere and the disk. Finally, the dimensionless Hersey parameter H is introduced as $H = \eta UR/F_n$.

3. Results and discussion

3.1. Pressure distribution and film thickness

In this Section, as focusing on the simple yet explicative sphere-on-disk scheme in Figure 1, we explore the influence that different contact configurations have, in the case of viscoelastic materials, on the pressure and film thickness distributions. In the model, the sphere radius is $R = 0.02$ m. As for the material, in the following analysis, in all the cases when we refer to the soft solids, we employ the same one relaxation time material with a glassy modulus $E_\infty = 10$ MPa, a ratio E_∞/E_0 equal to $E_\infty/E_0 = 100$ and a relaxation time $\tau = 0.01$ s. With regards to the lubricant, the fluid is iso-viscous with $\eta = 1$ Pa·s. Without loss of generality and for illustration purposes, all the calculations are carried out for a constant dimensionless normal load $F_n/\left(R^2 E_0\right) = 8.5\ 10^2$.

Now, by employing the aforementioned methodology, it is possible to focus on the different contact conditions. Let us start from the simple case, where the sphere is stationary, i.e., $\xi_b = 0$, and let us analyze what occurs in the three different configuration, that is, hard ball on soft layer (HS), soft ball on hard layer (SH), soft ball on soft layer (SS).

In Figure 3, in the three different cases, the deformed system at the centreline is shown: we refer, with dotted lines, to the undeformed solids-reported as reference for our analysis- , whereas, with the continuous lines, to the deformed surfaces. Calculations are carried out with the dimensionless speed $\xi_b = 0$ and $\xi_d = -0.21$: the resulting Hersey parameter H is $H = -1.26E - 04$. Now, in the HS case, where the ball is rigid, we are exactly in the case studied in Ref. (21): the sphere is, obviously, undeformed, while, due to viscoelasticity, the layer shows a non-symmetric deformation with smaller displacements at the leading edge, corresponding to the fluid inlet, and larger deformations at the trailing edge. Such an effect is well known in dry contact mechanics (25): indeed, at the trailing edge of a viscoelastic contact, the material has been deformed and, because of viscoelasticity, needs time to fully relax. When lubrication is considered, in the geometrical and motion configurations under investigation, nothing changes for the viscoelastic solid: at the flow inlet, i.e. where the lubricant is "sucked in", the viscoelastic material of the layer has not yet been indented; on the contrary, at the outlet, where the lubricant exits the contact region, the solid is still relaxing. Consequently, the layer leading edge corresponds to fluid inlet, and the trailing one to the fluid outlet.

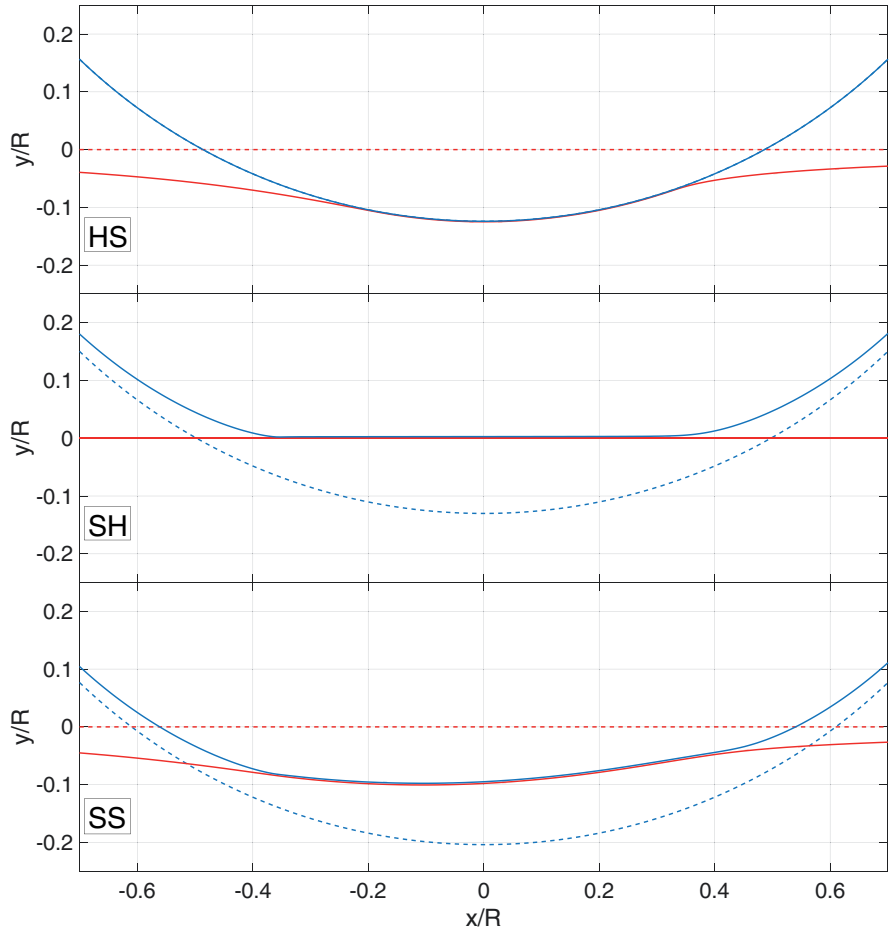

Figure 3: Deformed system at the centerline for the three different configurations: hard-on-soft (HS), soft-on-hard (SH) and soft-on-soft (SS). Red color refers to the sphere, blue to the layer. The dotted lines refer to the undeformed bodies, while the continuous lines are for the deformed surfaces. Calculations are carried out with the dimensionless speed $\xi_b = 0$ and $\xi_d = -0.21$: the resulting Hersey parameter H is $H = -1.26E-04$.

In the SH configuration, we have a very different outcome: here, only the sphere is deformable, but, as its speed is null, at the steady-state, no viscoelastic effect can occur and the sphere deforms with the rubbery modulus E_0 . The solution corresponds to what predicted by the classic elasto-hydrodynamic (EHL) theory. Finally, in the SS case, where both the sphere and the layer are deformed, the ball keeps on behaving elastically as its speed is null, whereas, in the layer deformation, there exist clear viscoelastic effects with a dissymmetry between the leading and the trailing edges. Interestingly, although the sphere is in the rubbery elastic regime, its deformation is not symmetric since the solid has to shape up with the viscoelastic layer below.

Figure 4 shows that, in the three cases, pressure distribution and film thickness are perfectly coherent with the deformed configurations in 3. Indeed, in the hard on soft contact (HS), we have a clear pressure peak at the leading edge due to the solid viscoelasticity: a correspondent minimum appears in the fluid film distribution. Furthermore, another minimum point occurs, then, at the fluid outlet for flow conservation. In the second configuration (SH), we have the classic iso-viscous EHL solution, whereas, in the last one (SS), a clear dissymmetry is present due to viscoelasticity, but, as the entire soft-on-soft system results more compliant, no pressure peak at the leading edge occurs. Indeed, as expected, the hard on soft case results the stiffest with larger values for the pressure distribution and smaller ones for the film thickness.

Contour maps in Figure 5 confirm the aforementioned trends. Indeed, in the SH configuration, the classic EHL contour maps, validated experimentally (the reader is referred, for example, to Ref. (1)), are found both in terms of pressure and fluid film. In the HS and SS configurations, viscoelasticity plays a major role with both the quantities showing a shape that is increasingly far from a circle and is affected by a sharp shrinkage at the fluid outlet, corresponding to the layer trailing edge. Incidentally, it can be observed that, because of the larger stiffness, the HS case shows a smaller contact region.

These results show how far viscoelastic lubrication may be from classic EHL. Ultimately, this is due to the different behaviour that occurs, when dealing with viscoelastic solids, between the leading and trailing edges of the contact region. However, things can become even more complicated. Indeed, this happens as soon as, in the soft on soft configuration, the sphere is allowed to move. In fact, in the previous analysis, ξ_b was null and, thus, the sphere behaved elastically; however, when we set a dimensionless speed

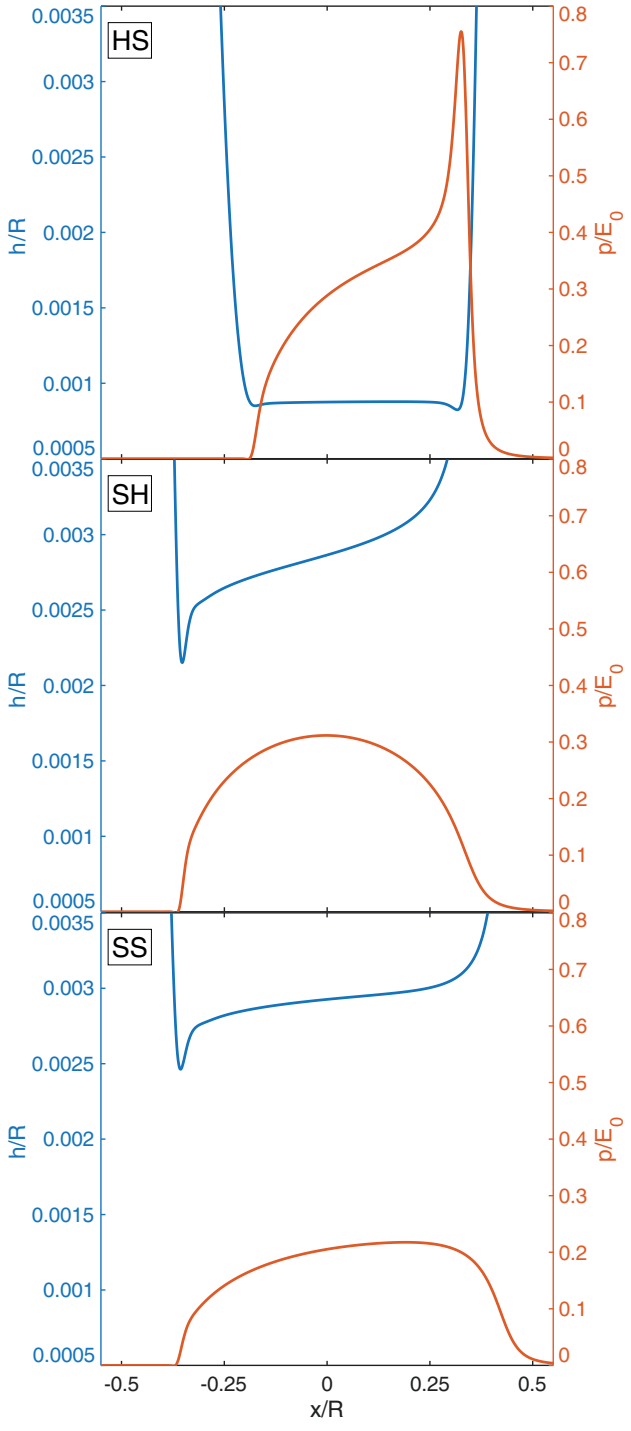

Figure 4: Film thickness (blue) and pressure distribution (red) at the centerline for the three different configurations: hard-on-soft (HS), soft-on-hard (SH) and soft-on-soft (SS). Calculations are carried out for $\xi_b = 0$ and $\xi_d = -0.21$: the resulting Hersey parameter H is $H = -1.26E-04$.

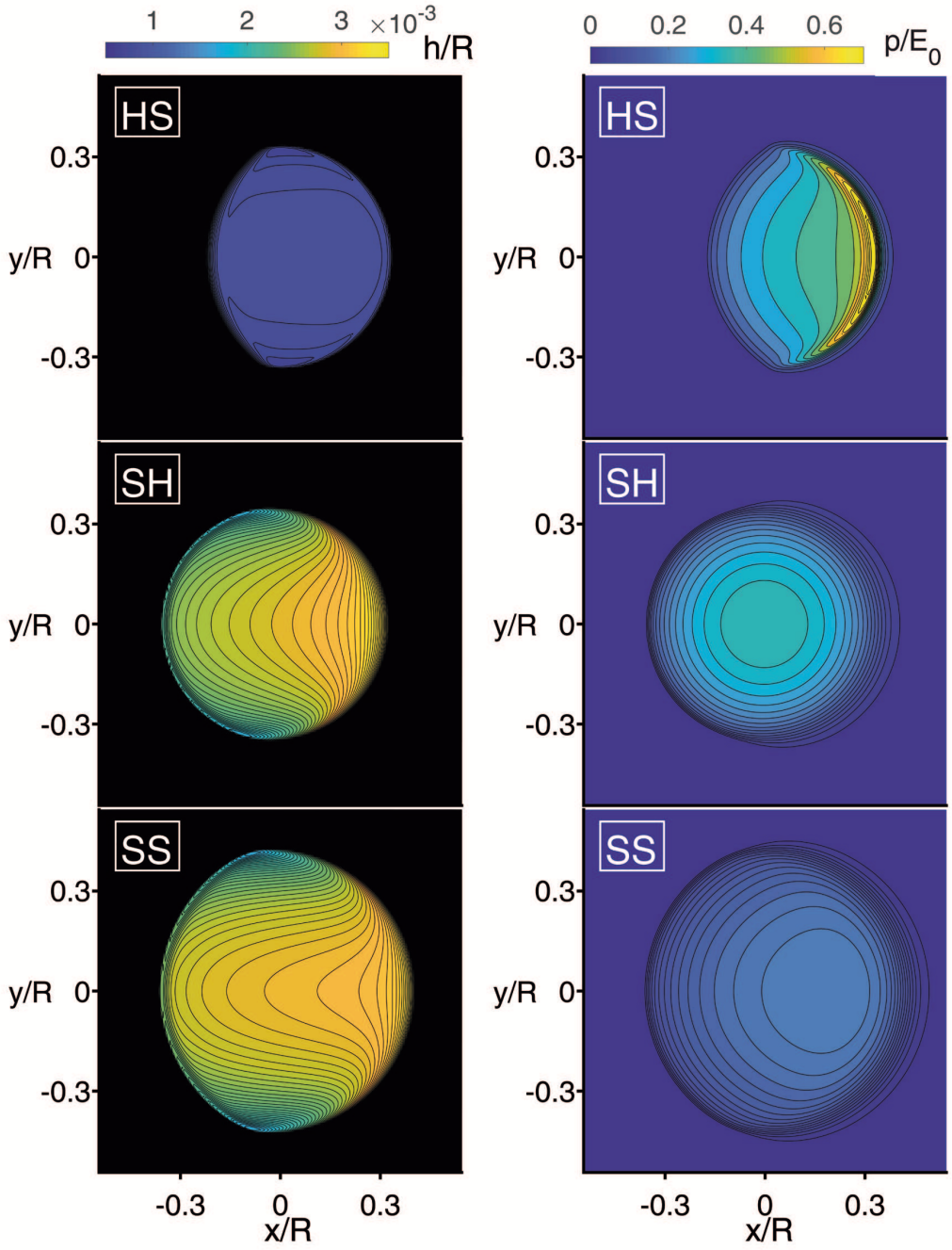

Figure 5: Contour plots for the film thickness (*left*) and pressure distribution (*right*) for the three different configurations: hard-on-soft (HS), soft-on-hard (SH) and soft-on-soft (SS). Calculations are carried out for $\xi_b = 0$ and $\xi_d = -0.21$: the resulting Hersey parameter H is $H = -1.26E - 04$.

ξ_b different from zero, the viscoelasticity effects on the sphere combine with those on the layer. Let us focus, in particular, on two possible soft on soft configurations. In the first one, defined SS_1, calculations are carried out for $\xi_b = 0.64$ and $\xi_d = -0.21$ with a resulting Hersey number $H = 2.5E-04$; in the second case, defined SS_2, the sphere and the layer speed ξ_b and ξ_d are set respectively to $\xi_b = -0.21$ and $\xi_d = -0.21$ and, thus, the resulting Hersey number is $H = -2.5E-04$. If we were in linear elastic conditions, the two cases would be perfectly specular with just the inlet and the outlet swapped by the sign of H. Conversely, in this study, things will be very different own to the viscoelasticity in the contacting bodies.

In the configuration SS_1, the leading edge of the viscoelastic layer is still at the right of the contact center, whereas the leading edge for the sphere is at the left side. The latter corresponds to the fluid inlet. This is clear in Figure 6, where the deformed system at the centreline is plotted. Incidentally, we notice that detecting, for each viscoelastic body, the leading region can be done easily by observing the zone where the material is stiffer and, thus, where the deformed surface is closer to the undeformed reference. In the configuration SS_2, at the right side of the contact center, we found both the sphere and the layer leading edge and the fluid inlet.

The difference between the configurations $SS_1$and SS_2 appears, then, evident in Figure 6 and is confirmed when we look at the pressure and fluid film distributions in Figure 7. We observe that, in the case SS_2, where the leading edges of the contacting solids coincide with the fluid inlet, we have a clear viscoelastic pressure peak and, thus, the corresponding minimum in the film thickness. In fact, as reported in the inset in Figure 7, the fluid film distribution shows two minimum points, one corresponding to the usual one due to flow conservation and the other related to the viscoelasticity. In the configuration SS_1, the outcome is more complicated due to the different position of the leading edge for each viscoelastic body. Specifically, the interplay between the viscoelastic effects in the solids produces a larger film with a corresponding pressure distribution spreading over the contact region.

These trends are perfectly coherent with the contour maps in Figure 8 where we plot pressure distribution and film thickness in the two cases $SS_1$and SS_2. Particularly interesting is the configuration SS_1, which shows a marked stretch, for both the distributions, perpendicularly to the speed. Indeed, we clearly detect the fluid inlet, but no contact leading edge can be found as, conversely, in the configuration SS_2. In the latter, we clearly identify the usual shrinkage appearing, in the trailing zone, for a viscoelastic contact.

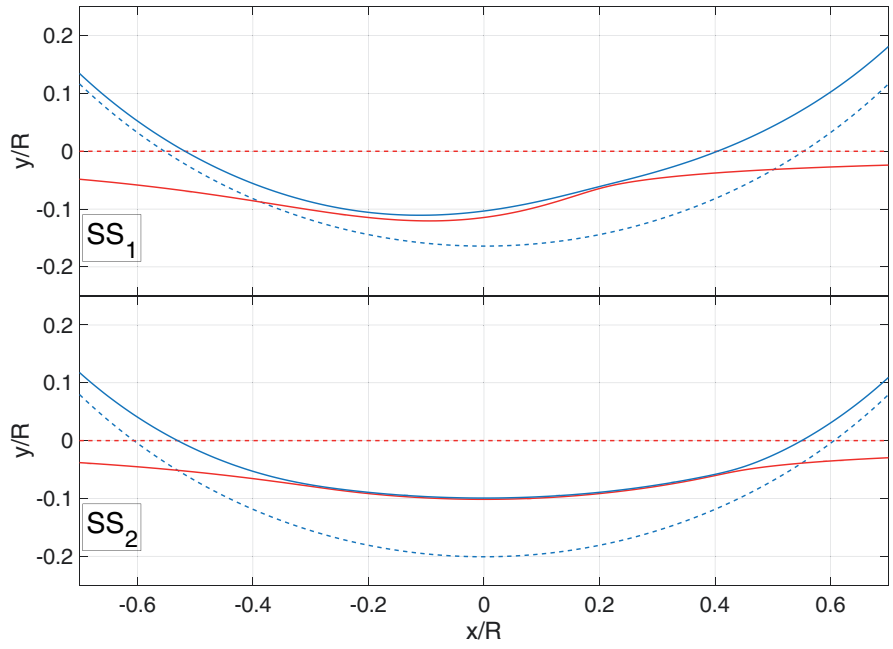

Figure 6: Deformed system at the centerline for two different soft-on-soft configurations: in the first one, SS_1 , calculations are carried out for $\xi_b = 0.64$ and $\xi_l = -0.21$ and, thus, the Hersey number $H = 2.5E-04$; in the second one, SS_2 , calculations are conducting with $\xi_b = -0.21$ and $\xi_l = -0.21$ and, thus, the Hersey number $H = -2.5E-04$. The dotted lines refer to the undeformed bodies, while the continuous lines are for the deformed surfaces.

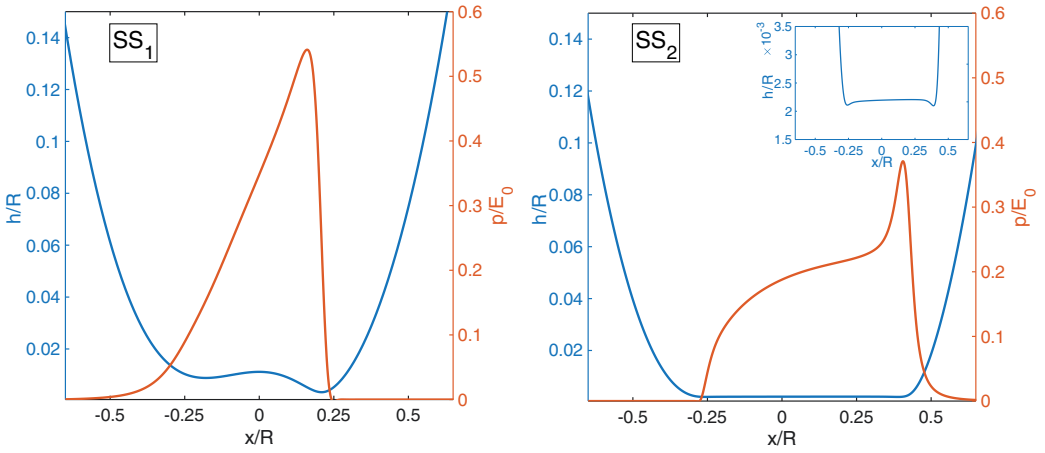

Figure 7: Film thickness (blue) and pressure distribution (red) for two different soft-on-soft configurations: in the first one, SS_1 , calculations are carried out for $\xi_b = 0.64$ and $\xi_l = -0.21$ and, thus, the Hersey number $H = 2.5E-04$; in the second one, SS_2 , calculations are conducting with $\xi_b = -0.21$ and $\xi_l = -0.21$ and, thus, the Hersey number $H = -2.5E-04$. In the latter, the inset shows a zoom of the film thickness.

Ultimately, the crucial point here is that, in soft lubricated contacts, where both the contacting bodies have a viscoelastic rheology, the phenomenon is governed not only by the Hersey parameter H , but also by the dimensionless velocities ξ_b and ξ_d . This effect cannot be embedded in classic theory of elasto-hydrodynamic lubrication and must be explained by accounting for the solid viscoelasticity.

3.2. Friction

When considering the friction force associated to lubricated soft contacts, as shown in Ref. (21), it is necessary to account for the viscoelastic hysteresis, in addition to the viscous losses. Consequently, the relation between friction and entrainment speed cannot be reduced to the classic trends predicted by the Stribeck curve and, thus, by the empirically obtained laws proposed in the past decades (1).

In this paper, we compare the outcomes of our methodology with the experimental results recently published in Ref. (23). Here, a ball-on-disk tribometer is employed to test viscoelastic lubrication in three different configuration, that is, hard ball on soft layer (HS), soft ball on hard layer (SH), soft ball on soft layer (SS). The sphere is always stationary. These exper-

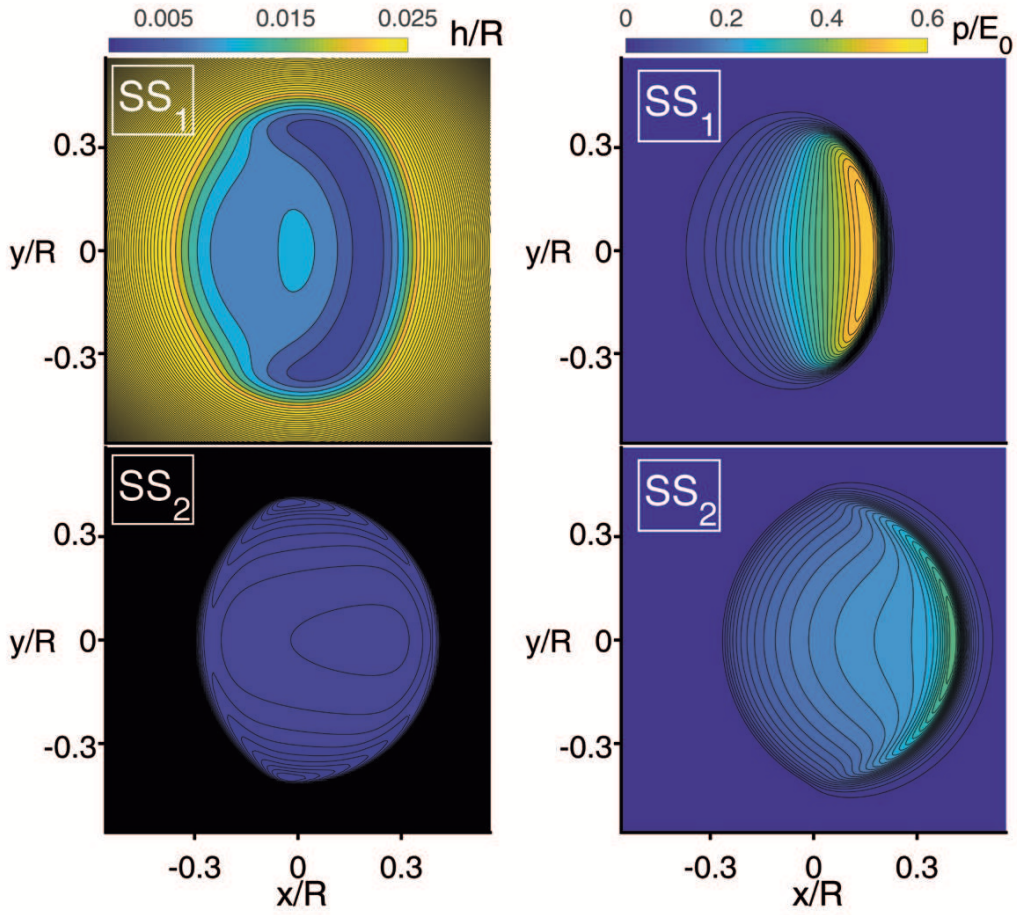

Figure 8: Contour plots for the film thickness (*left*) and pressure distribution (*right*) for the three different configurations: for two different soft-on-soft configurations: in the first one, SS_1 , calculations are carried out for $\xi_b = 0.64$ and $\xi_l = -0.21$ and, thus, the Hersey number $H = 2.5E-04$; in the second one, SS_2 , calculations are conducting with $\xi_b = -0.21$ and $\xi_l = -0.21$ and, thus, the Hersey number $H = -2.5E-04$. The dotted lines refer to the undeformed bodies, while the continuous lines are for the deformed surfaces.

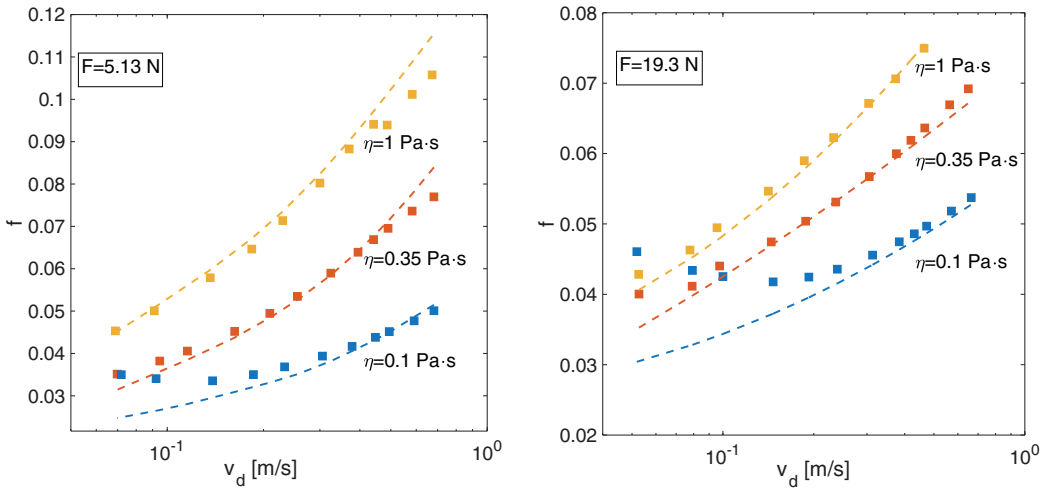

Figure 9: Friction coefficient as a function of the disk speed u_d for different values of viscosity η and for two values of the normal load, that are $F_n = 5.13$ N (*on the left*) and $F_n = 19.3$ N (*on the right*). Data refer to the hard on soft configuration, i.e., to the contact of a steel ball with a NBR layer. Dotted lines show numerical results, whereas points are the exprimental outcomes.

imental results have shown that, in the cases (HS) and (SS), viscoelastic hysteresis plays a fundamental role and has to be taken into account when considering the overall lubricated friction.

Let us focus first on the hard on soft configuration (HS). Specifically, a steel ball is into contact with a nitrile butadiene rubber (NBR) disk. For the viscoelastic characterization of such a material, carried out by means of the Dynamic Mechanical Analysis (DMA), the reader is referred to Ref. (23).

In Figure 9, we compare numerical results and experiments for two levels of normal load, i.e., $F_n = 5.13$ N and $F_n = 19.3$ N , and for three different lubricants, with viscosity respectively being equal to $\eta = 0.1$Pa·s , $\eta = 0.35$ Pa·s , $\eta = 1$Pa·s . As noticed above, unlike classic EHL, in lubrication of viscoelastic solids, viscosity and sliding velocities have to be considered independently: thus, we plot the friction coefficient as a function of the disk speed for different values of η . We observe a good agreement between theory and experiments in a wide range of speed values; however, the reliability of numerical predictions deteriorates for low values of the speed and viscosity. This is due to the transition between a fully developed lubrication regime and a mixed regime, where roughness plays a major role. Accounting for the

surface roughness is out of the scope of this work, but let us notice that, as expected, the transition to mixed lubrication becomes more marked when increasing the load. Interestingly, when far from the mixed regime, also for the highest level of load, numerical results agrees with experiments, thus showing that material non-linearities have a negligible influence.

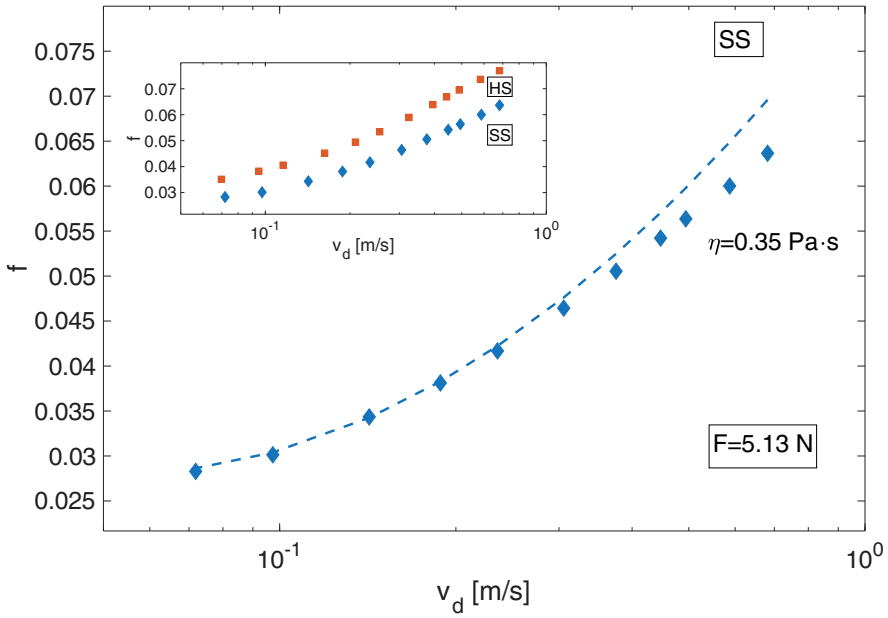

Figure 10: Friction coefficient as a function of the disk speed u_d for different values of viscosity η and for a normal load equal to $F_n = 5.13$ N . Data in the main plot refer to the soft on soft configuration, i.e., to the contact of a NBR ball with a NBR layer. In the inset, we compare the experimental data in the such a configuration with the hard on soft case. Dotted lines show numerical results, whereas points are the exprimental outcomes.

Now, Figure 10 shows the friction as function of the speed for the soft on soft configuration. Experimental results have been obtained in Ref. (23) by putting in contact a NBR ball with a NBR disk. First of all, we should pay attention to the inset where, for the same level of load and viscosity, we plot experimental data for the hard on soft and the soft on soft configurations: as the latter is more compliant than the first contact case, it entails smaller values for the friction coefficient. Regarding the comparison between experimental data and numerical outcomes, we observe also in this case a good agreement, thus confirming the generality of the numerical approach

proposed in this paper.

4. Conclusion

In this paper, we focus on the role played by a linear viscoelastic rheology on determining the lubrication of soft solids. Specifically, this study is aimed at showing how viscoelasticity modifies, in comparison with the classic elasto-hydrodynamic theory, all the quantities that characterize lubrication, including pressure, film thickness and friction.

To this end, a generalized mathematical formulation has been developed to deal with the lubricated contact between linearly viscoelastic solids: a finite difference solver, implemented to tackle the Reynolds equations, has been coupled with a boundary element methodology capable of determining the solid deformations in each of the bodies into contact. In order to elucidate the phenomenon, we have studied a simple yet explicative tribo-system, that is, the lubrication between a sphere and a layer, as in a ball-on-disk tribometer. Crucially, results show the significance of the contact configuration in determining the system outcomes. Indeed, if the sphere is stationary, in the soft on hard configuration (SH), i.e., a soft ball into contact with a hard disk, the classic EHL regime is found as the sphere does not move and, thus, behaves elastically. Conversely, in the hard on soft configuration (SH), there occurs the visco-elasto-hydrodynamic regime (VEHL) defined in Ref. (21): the lubricating film reveals a marked shrinkage at the fluid outlet with a possible additional minimum point at the inlet, where the pressure distribution presents a peak. Finally, in the soft-on-soft case (SS), a complex interplay between the two solids viscoelasticity and the fluid viscosity is shown. Things complicate when, in the latter configuration, the sphere is allowed to move. Ultimately, we have to point out that, in order to fully assess viscoelastic lubrication, three parameters have to be considered. Specifically, in addition to the Hersey number H, commonly included in lubrication theory, the dimensionless velocities for the sphere and the layer, $\xi_b = v_b\tau/R$ and $\xi_{\mathbf{d}} = v_d\tau/R$, have to be accounted for, as they determine, each independently from the other one, the viscoelastic behaviour of the sphere and the layer.

Viscoelastic lubrication has, finally, a direct impact also on friction: results show a significant deviation from conventional Stribeck curve and a marked dependence on the contact configuration. Comparison between numerical outcomes and experimental tests shows a good agreement, thus contributing to validate the proposed numerical methodology.

Acknowledgements

CP thanks Prof. Stupkiewicz and Dr. Sadowski for providing the experimental data employed in this paper and for useful discussions on the topic. Furthermore, the support of CeMec (Polytechnic University of Bari), in terms of access to computational facilities, is acknowledged.

[1] Hamrock B. J., Schmid S.R., Jacobson B. O. Fundamentals of Fluid Film Lubrication, CRC Press, (2004).

[2] Bowden F. P., Tabor D., The Friction and Lubrication of Solids, Clarendon Press, (2001).

[3] Ahn B. K. , Lee D. W., Israelachvili J. N., Waite J. H. Surface-initiated self-healing of polymers in aqueous media. Nature Materials, 13, 867–872 (2014).

[4] Rus D. and Tolley M. T. Design, fabrication and control of soft robots. Nature 521, 467–475, (2015).

[5] Olabisi O., Adewale K. Handbook of Thermoplastics . CRC Press, (2016).

[6] Bao G. , Suresh S. Cell and molecular mechanics of biological materials. Nature Materials, 2, 715 - 725, (2003).

[7] Licup A. J., Münster S., Sharma A., Sheinman M., Jawerth L. M., Fabry B., Weitz D. A., MacKintosh F. C. Stress controls the mechanics of collagen networks. PNAS,112 ,31, (2016).

[8] Heepe L. and Gorb S. N. Biologically Inspired Mushroom-Shaped Adhesive Microstructures. Annual Review of Materials Research, 44:173–203, (2014).

[9] Endlein T., Barnes W. J. P., Samuel D. S., Crawford N. A. , Biaw A. B., Grafe U. Sticking under Wet Conditions: The Remarkable Attachment Abilities of the Torrent Frog, Staurois guttatus. PLoS ONE 8, e73810 (2013).

[10] André T. , Lévesque V., Hayward V. , Lefèvre P. , Thonnard J.-L. Effect of skin hydration on the dynamics of fingertip gripping contact, Journal of the Royal Society Interface, 8, 64, (2011).

[11] Persson B.N.J., Albohr O., Tartaglino U., Volokitin A. I., Tosatti E. On the nature of surface roughness with application to contact mechanics, sealing, rubber friction and adhesion. Journal of Physics: Condensed Matter, 17, 1, (2004).

[12] Vlădescu SC , Putignano C , Marx N ,Keppens T , Reddyhoff T , Dini D . The Percolation of Liquid Through a Compliant Seal—An Experimental and Theoretical Study, Journal of Fluids Engineering 141 (3), 031101, (2019).

[13] Dapp, W.B., Lücke, A., Persson, B.N.J., Müser, M.H. Self-affine elastic contacts: Percolation and leakage, Physical Review Letters, 108 (24), 244301, (2012).

[14] Shukla A. and Datta T., Optimal use of viscoelastic dampers in building frames for seismic force, J. Struct. Eng. 125, 401 (1999).

[15] You-Qiang Wang, Xiu-Jiang Shi, Li-Jing Zhang, Experimental and numerical study on water-lubricated rubber bearings, Industrial Lubrication and Tribology, 66, 2, 282-288, (2014).

[16] Kim J ,Chung SE , Choi SE , Lee, Kim J , Kwon S , Programming magnetic anisotropy in polymeric microactuators - Nature materials, 2011.

[17] Johnson K.L.J., Contact Mechanics, Cambridge University Press (1985).

[18] Venner C.H. and Lubrecht A.A., Multilevel Methods in Lubrication, Elsevier Tribology Series, Ed. D. Dowson et al., V. 37, (2000).

[19] Snoeijer J. H. , Eggers J. , Venner C. H. . Similarity theory of lubricated Hertzian contacts. Physics of Fluids, 25(10):101705, (2013).

[20] Scaraggi M. and Persson B.N.J. Theory of viscoelastic lubrication, Tribology International, 118–130, 72, (2014).

[21] Putignano C.,Dini D. , Soft matter lubrication: does solid viscoelasticity matter?, ACS Applied Materials & Interfaces, 9 (48), 42287-42295, (2017).

[22] Selway N., Chana V., Stokes J. R. Influence of fluid viscosity and wetting on multiscale viscoelastic lubrication in soft tribological contacts, Soft Matter, 8, (2017).

[23] Stupkiewicz S., Lengiewicz J., Sadowski P., Kucharski S., Finite deformation effects in soft elastohydrodynamic lubrication problems, Tribology International, 511–522, 93, (2016).

[24] Hunter S.C. The rolling contact of a rigid cylinder with a viscoelastic half space . Transactions of ASME, Series E, Journal of Applied Mechanics, 28, 611–617 (1961).

[25] Carbone G. , Putignano C., A novel methodology to predict sliding/rolling friction in viscoelastic materials: theory and experiments. Journal of the Mechanics and Physics of Solids, 61 (8), 1822-1834, (2013).

[26] Putignano C. , Carbone G. , Dini D. , Theory of reciprocating contact for viscoelastic solids. Physycal Review E 93, 043003, (2016).

[27] Grosch K. A. , The Relation between the Friction and Visco-Elastic Properties of Rubber, Proceedings of the Royal Society of London. Series A, Mathematical and Physical, 274-1356, 21-39, (1963).

[28] Putignano C., Reddyhoff T., Carbone G., Dini D. Experimental investigation of viscoelastic rolling contacts: a comparison with theory. Tribology Letters , 51, 105–113, (2013).

[29] Hooke CJ, HuangP. , Elastohydrodynamic lubrication of soft viscoelastic materials in line contact. Proceedings Institutions of Mechanical Engineering Part J: Journal of Engineering Tribology 211:185, (1997).

[30] Elsharkawy AA. Visco-elastohydrodynamic lubrication of line contacts. Wear. 199:45–53. (1996).

[31] Koumi K. E., Chaise T., Nelias D., Rolling contact of a rigid sphere/sliding of a spherical indenter upon a viscoelastic half-space containing an ellipsoidal inhomogeneity, Journal of the Mechanics and Physics of Solids, 80, 1–25, (2015).

[32] Koumi KE,Nelias D ,Chaise T , Duval A, Modeling of the contact between a rigid indenter and a heterogeneous viscoelastic material, Mechanics of Materials 77, 28-42, (2014).

[33] Pandey A., Karpitschka S., Venner C. H., and Snoeijer J. H. Lubrication of soft viscoelastic solids. Journal of Fluid Mechanics, 799:433–447, (2016).

[34] Marx N, Guegan J, Spikes H.A. Elastohydrodynamic film thickness of soft EHL contacts using optical interferometry, Tribology International, 99, 267-277, (2016).

[35] Hutt W. and Persson B. N. J. , Soft matter dynamics: Accelerated fluid squeeze-out during slip, The Journal of Chemical Physics 144, 124903, (2016).

[36] Putignano C., Afferrante L.,Carbone G., Demelio G. A new efficient numerical method for contact mechanics of rough surfaces. International Journal of Solids and Structures, 49 (2), (2012).

[37] Putignano C., Afferrante L. , Carbone G., Demelio G. The influence of the statistical properties of self-affine surfaces in elastic contact: a numerical investigation, Journal of Mechanics and Physics of Solids, 60, 5, 973–982, (2012).

[38] Putignano C. , Carbone G., Dini D. Theory of reciprocating contact for viscoelastic solids. Physycal Review E 93, 043003, (2016).

[39] Christensen R. M., Theory of viscoelasticity,Academic Press, New York, (1971).

[40] M.L. Williams, R.F. Landel, J.D. Ferry, J. Amer. Chem. Soc., 77:3701, (1955).

[41] Carbone G., Mangialardi L. Adhesion and friction of an elastic half-space in contact with a slightly wavy rigid surface, Journal of the Mechanics and Physics of Solids, **52** (6), 1267-1287, (2004).

[42] Putignano C., Carbone G., Dini D., Mechanics of Rough Contacts in Elastic and Viscoelastic Thin Layers, International Journal of Solids and Structure, 69–70, 507–517, (2015).

[43] Putignano C. ,Dapp W. and Muser M. A GFMD approach to the mechanical contact between thin elastic sheets and randomly rough surfaces , Biomimetics 1 (1), 7,(2016).

[44] Schenk O. and Gärtnerc K., Solving unsymmetric sparse systems of linear equations with PARDISO, Future Generation Computer Systems, 20, 3, 475–487, (2004).

[45] Esfahanian M. & Hamrock B. J., Fluid-Film Lubrication Regimes Revisited, Tribology Transactions, 34,4, 628-632, (1991).